

**Synergistic phonon scattering in epitaxial silicon multilayers with germanium nanodot inclusions**Takafumi Oyake,<sup>1</sup> Lei Feng,<sup>1</sup> Makoto Kashiwagi,<sup>2</sup> Takuma Shiga<sup>1</sup>,<sup>1</sup> Takuma Hori<sup>1</sup>,<sup>3</sup> Suto Yamasaka,<sup>4</sup> Yoshiaki Nakamura,<sup>4</sup> and Junichiro Shiomi<sup>1,\*</sup><sup>1</sup>*Department of Mechanical Engineering, The University of Tokyo, 7-3-1 Hongo, Bunkyo-ku, Tokyo 113-8656, Japan*<sup>2</sup>*Department of Chemistry and Biological Science, Aoyama Gakuin University, 5-10-1 Fuchinobe, Chuo-ku, Sagami-hara, Kanagawa 252-5258, Japan*<sup>3</sup>*Department of Mechanical Systems Engineering, Tokyo University of Agriculture and Technology, 2-24-16 Nakacho, Koganei, Tokyo 184-0012, Japan*<sup>4</sup>*Graduate School of Engineering Science, Osaka University, 1-3 Machikaneyama, Toyonaka, Osaka 560-8531, Japan*

(Received 27 February 2021; revised 10 June 2021; accepted 20 July 2021; published 16 August 2021)

Temperature-dependent thermal conductivity of epitaxial silicon (Si)/ultrathin silica multilayers film with epitaxial germanium (Ge) nanodot inclusions is measured over the range of temperature from 50 K to room temperature using time-domain thermoreflectance. The measured thermal conductivity with 5-nm Ge nanodots is much smaller than the reported values for Si/Ge superlattices, bulk SiGe, and nanostructured SiGe in the entire temperature range. The thermal conductivity of the film is analyzed with a kinetic model incorporating multiple phonon scattering processes, where intrinsic three-phonon scattering inside the Si layers is calculated by first principles, boundary scattering at the ultrathin silica layer is calculated by the atomistic Green's function, and scattering by the Ge nanodots is approximated with nanovoids. The analysis reveals that summing the multiple scattering rates by Matthiessen's rule cannot explain the extremely low thermal conductivity. The Monte Carlo ray tracing calculation that incorporates the multiple scattering effect reveals that the synergistic effect of ultrathin silica interfaces and Ge nanodots enhances phonon scattering. This suggests the merit in synergistically designing multiple nanostructures to reduce thermal conductivity, which is beneficial for developing thermoelectric materials.

DOI: [10.1103/PhysRevB.104.054301](https://doi.org/10.1103/PhysRevB.104.054301)**I. INTRODUCTION**

Thermoelectric (TE) generators that can directly convert heat to electricity [1–3] are thought to be a key future technology for energy harvesting. However, the spread of application requires further enhancement in material conversion efficiency, i.e., a higher figure of merit,  $ZT = S^2\sigma T/\kappa$ , where  $S$  is the Seebeck coefficient,  $\sigma$  is electrical conductivity, and  $\kappa$  is thermal conductivity, at a given temperature  $T$ . Conventional materials to this date are  $\text{Bi}_2\text{Te}_3$  [4] and  $\text{PbTe}$  [5] in forms of alloys and nanostructures; however, these materials with heavy elements have limitations in terms of cost and safety, and thus there is increasing interest in engineering materials consisting of abundant and environment-friendly elements. Crystal silicon (Si) is a representative material of such but it has relatively low  $ZT$  due to high thermal conductivity despite its high power factor ( $S^2\sigma$ ) when properly doped. There have recently been a growing number of works aiming to reduce  $\kappa$  of Si TE materials by nanostructuring and this has greatly advanced their  $ZT$  [6–15]. A widely studied class of the nanostructured materials is nanocrystalline Si synthesized by sintering nanoparticles prepared by ball milling [13] or plasma-enhanced chemical vapor deposition [16]. In the nanocrystalline structures, phonons propagate ballistically

inside the nanometer-size grains and are scattered at dense grain boundaries, resulting in a large reduction of  $\kappa$  from the value of a single crystal.

Further enhancement of  $ZT$  requires more precise control of the grain geometry/crystallinity and interfacial physical/chemical structures. Aiming at realizing the controllability, Si film composed of epitaxially and coherently connected Si-nanocrystal grains with identical crystal orientations was synthesized [17]. There, grains as small as 3 nm in diameter are separated by monolayer (ML)  $\text{SiO}_2$  but are connected through nanowindows, enabling coherent connection between the grains with the same crystal orientation. The nanostructured crystal Si has been shown to realize extremely small thermal conductivity even below that of amorphous Si, by the  $\text{SiO}_2$  interfacial layer ultimately reducing the mean free paths of acoustic phonons to the minimum heat conduction scenario [18].

To improve electrical conductivity maintaining low thermal conductivity, Ge nanodots (GeNDs) were introduced, where epitaxial Si multilayers separated again with ML  $\text{SiO}_2$  but this time with ultrasmall epitaxial GeND inclusions (hereafter called Si/GeND nanostructure) [19]. Here, GeNDs were epitaxially grown on the  $\text{SiO}_2$  layer, but are connected with the Si on the other side of the  $\text{SiO}_2$  layer through the nanowindow [20], allowing electrons to conduct. The GeNDs are much smaller than those previously obtained by the Stranski-Krastanov (SK) growth mode, and the interface between

\*shiomi@photon.t.u-tokyo.ac.jp

TABLE I. Sample details. Ge and Si are formed alternately eight times to obtain the Si/GeND structure. The lateral dot size and sample thickness are measured by transmission electron microscopy, and the areal density of the Ge nanodots is measured by scanning tunneling microscopy.

Sample name	Total thickness (nm)	Thickness of each layer (nm)	Number of layer repetitions	Lateral dot size (nm)	GeNd areal density ( $10^{10} \text{ cm}^{-2}$ )	Ge fraction (%)
5-nm NDs	62.5	7.81	8	5	138	12.3
40-nm NDs	208	26.0	8	40	3.2	34.9
13-nm NDs	353	44.1	8	13	24.2	6.2

the embedded GeNDs and the Si matrix is clean with little interfacial mixing, and no strains nor misfit dislocations [20–22]. The resulting thermal conductivity of the Si/GeND nanostructure was lower than those of the other conventional SiGe materials and the GeND/Si superlattice obtained by SK growth mode at room temperature. As for the electron properties [23], with proper doping (electron concentration of  $10^{19}$ – $10^{20} \text{ cm}^{-3}$ ), electron mobility of the Si/GeND nanostructure ( $30$ – $60 \text{ cm}^2 \text{ V}^{-1} \text{ s}^{-1}$ ) is close to those of epitaxial Si film ( $40$ – $70 \text{ cm}^2 \text{ V}^{-1} \text{ s}^{-1}$ ) and its Seebeck coefficient is  $-200$  to  $-250 \mu\text{V K}^{-1}$  at an electron concentration of around  $10^{19} \text{ cm}^{-3}$ , which agrees with those of epitaxial Si film ( $-200$  to  $-300 \mu\text{V K}^{-1}$ ) [24]. This demonstrates that the Si multilayer with GeND can independently control phonons and carrier transport.

Although extremely low thermal conductivity has been achieved in the Si/GeND nanostructure, little is known about the mechanism of how phonons are efficiently scattered by GeND and ML  $\text{SiO}_2$  interfaces. The key question is whether there is interplay between GeND and ML  $\text{SiO}_2$  for phonon scattering. Both GeND and ML  $\text{SiO}_2$  scatter phonons but if the two events are independent, the total scattering rate will be the sum of the two scattering rates as in Matthiessen’s rule. Such approximation has been applied and shown to be sufficient in many composites with multiple kinds of scatterers [7,24,25]. However, this may not be the case when the characteristics of the different scatterers are significantly different. Identifying these aspects requires quantitative analysis of phonon transport from a microscopic viewpoint. In this work, we have achieved it by measuring the temperature dependence of thermal conductivity of the Si/GeND nanostructure by the time-domain thermoreflectance (TDTR) method over the range of temperature from 50 K to room temperature, and performing theoretical calculations combining a kinetic model based on first-principles calculation, phonon Monte Carlo ray tracing, and atomistic Green’s function methods. Demonstration of the presence of the synergistic effect between GeND and ML  $\text{SiO}_2$  would serve to open a route to reduce thermal conductivity.

## II. SAMPLES AND THERMAL CONDUCTIVITY MEASUREMENTS

The synthesis process of Si/GeND nanostructures in the form of thin films is described in previous works [19,23]. The properties of the GeNDs nanostructure are shown in Table I. The number density of GeNDs is measured by using scanning tunneling microscopy. Here, for instance, we refer to the

sample using the lateral GeND size as a “5-nm GeND sample,” although the thickness of the Si layer also varies with samples.

Figure 1(a) shows schematics of the Si/GeND nanostructure covered by an Al thin film as a transducer for TDTR measurement [26]. Figure 1(b) shows the cross-sectional bright-field scanning transmission electron microscopy (TEM) image of 13-nm GeND/Si samples. The TEM image shows the periodic structures of GeNDs (dark contrast) and a Si thin layer (bright contrast). In contrast to the GeNDs obtained by the SK growth mode, which typically have a pyramid shape with sizes ranging from 30 to 100 nm, the GeNDs in this study are hemispherical and much smaller. In addition, since the Si surface is covered by ML  $\text{SiO}_2$  instead of a Ge thin film, GeNDs in this study are completely different from SK GeNDs. See Refs. [19,23] for more details of the structures.

The thermal conductivity of the Si/GeND nanostructure was measured by the TDTR method [26,27] with a modulation frequency of 11 MHz. For the fitting process, the heat capacity of Al and Si is taken from the literature [18], and the Si/GeND nanostructure is estimated from the ratio of Si and Ge in the molecular beam epitaxy process. The thermal boundary conductance at the interface between Al and Si/GeND and the thermal conductivity of the silicon substrate are determined by performing TDTR measurement on a reference sample, consisting of a Si substrate with native oxide coated by an Al thin film (thickness of  $\sim 80$  nm), in the same temperature range. The interface conductance between the Si/GeND film and the Si substrate, for the sake of simplicity, is included in the Si/GeND thermal conductivity considering ML  $\text{SiO}_2$  at the interface as a part of the film. Note that the sensitivity of the TDTR signal to the thermal boundary conductance is small, and thus whether to include it in the Si/GeND thermal conductivity has minor impact on the resulting value. Details of how to analyze the parameter sensitivity of the TDTR signal are described elsewhere [28]. The remaining parameters are thicknesses of the Al layer and the Si/GeND sample. For the Al-layer thickness, another reference sample with the Al thin film deposited on a quartz substrate was prepared in the same batch as the Si/GeND sample, and TDTR measurement was performed to identify the Al-layer thickness though acoustic echo and also by fitting the ratio signal with the thickness as a parameter. The thickness of the Si/GeND film was determined from the TEM images with an uncertainty of 5%. Low temperature measurements were taken with the cryostat chamber under high vacuum ( $1 \times 10^{-4}$  Pa).

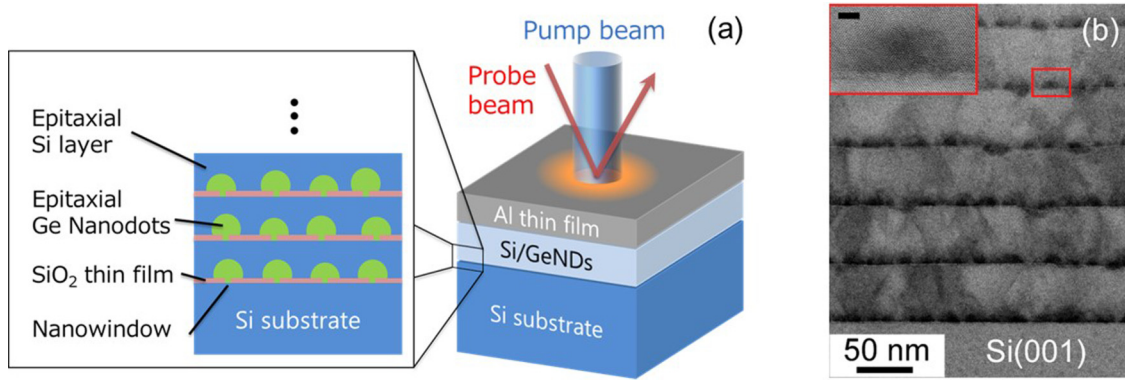


FIG. 1. (a) A schematic of TDTR measurement of the Si/GeND structure. The Si/GeND structure is grown on a Si substrate and covered by an Al thin film ( $\sim 80$  nm thick) as a transducer layer for TDTR measurement. (b) Cross-sectional bright-field scanning transmission electron microscopy image of 13-nm Ge nanodots/Si samples. The inset in (b) is an enlarged image of the solid rectangular marked region in (b). Dark and bright contrasts correspond to Ge and Si, respectively. In the inset, scale bars correspond to 3 nm.

Figure 2 shows the TDTR measurement of the cross-plane thermal conductivity of Si/GeND structures with respect to temperature. The values of the Si/Ge superlattice, bulk SiGe, and nanostructured SiGe are also plotted for comparison [29].

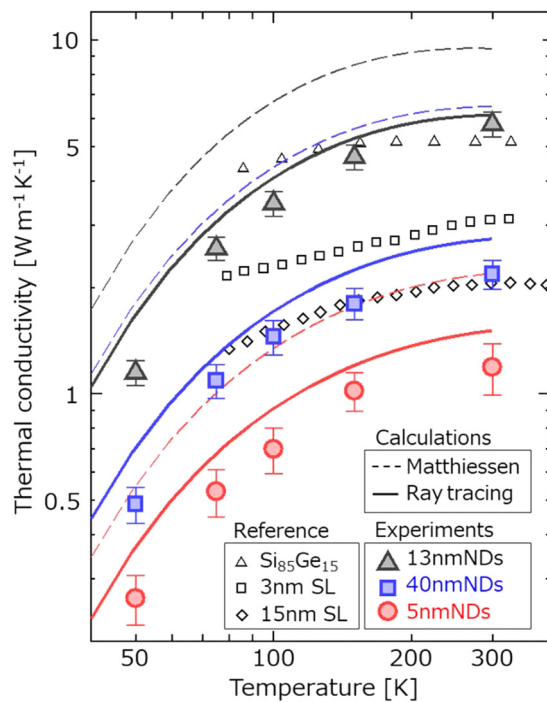


FIG. 2. Thermal conductivity of 5-nm ND (circle), 13-nm ND (triangle), and 40-nm ND (square) samples as a function of temperature. The filled symbols are the experimentally measured data. The dashed and solid lines represent the calculated thermal conductivity with effective mean free path obtained by using Matthiessen's rule for superlattice scattering ( $\Lambda_{SL}$ ) and particle scattering ( $\Lambda_{Ge}$ ), and by Monte Carlo ray tracing simulation for Si/GeND structures, respectively. The open symbols represent the thermal conductivity of a  $\text{Si}_{85}\text{Ge}_{15}$  thin film, and a Si/Ge superlattice with superlattice periods 3 and 15 nm, taken from Ref. [29], respectively.

The thermal conductivity of the current measurement at room temperature ( $1.2 \text{ W m}^{-1} \text{ K}^{-1}$ ) agrees well with previously reported values measured by the  $2\omega$  method [19]. In comparison with Si/Ge alloys, nanostructured SiGe with similar Ge volume fraction, and a SiGe superlattice, the thermal conductivity of the Si/GeND structure is much lower in the entire temperature range. While the thickness of each Si layer is different in the three samples, the trend of the temperature dependence of thermal conductivity is similar. This suggests that the thermal conductance of the Si/GeND film is insensitive to the intrinsic thermal resistance of each Si layer, which is understandable as phonons are expected to ballistically transport inside the Si layer. Therefore, the thermal conductance and temperature dependence of the structure are determined by the interfacial resistance, as indicated in Ref. [19].

The results demonstrate that the Si/GeND samples exhibit a lower thermal conductivity with smaller Ge fraction ( $\sim 10\%$ ) than those of the other conventional SiGe materials with a Ge fraction of 20% [11,12]. Alternatively, the thermal resistance (total thickness of Si/GeNDs divided by its thermal conductivity) strongly depends on the GeND size and number density, indicating that the thermal resistance is dominantly determined by the GeND morphology, and is independent of the geometry of the Si layer. This is beneficial when considering decoupling phonon and electron transport for thermoelectric application since the geometry of the Si layer influences electron transport. Furthermore, the thermal resistance of the current sample is larger than that of the SK ND superlattice, estimated from the reports by Pernot *et al.* ( $2\text{--}4 \times 10^{-9} \text{ m}^2 \text{ K W}^{-1}$ ) [30], indicating the effectiveness of the present GeNDs. The existence of stacking faults in the samples should also be considered as a possible source of thermal resistance. However, the effect of the stacking faults is very small ( $\sim 30\%$   $\kappa$  reduction in bulk fcc crystals) [29] compared with the present reduction in  $\kappa$ . Therefore, stacking faults are unlikely to be the main cause of the reduction in  $\kappa$ . This result shows that the proposed stacked structures reduce thermal conductivity the most effectively in the various SiGe materials studied.

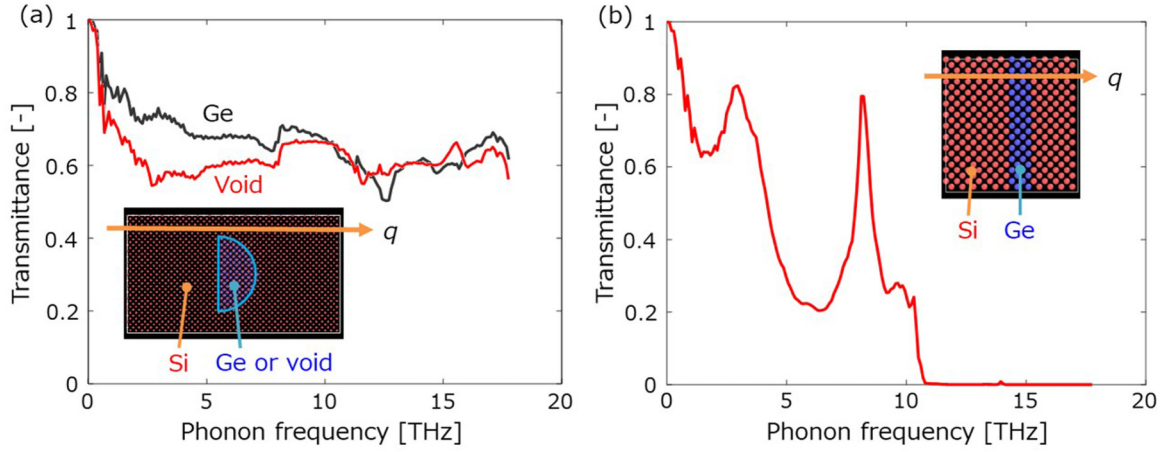


FIG. 3. Phonon transmittance of nanostructure calculated by AGF. (a) Phonon transmittance for a Ge hemisphere (blue dots in inset, 3.258 nm in diameter) embedded in Si (red dots in inset) crystals. The cross section of the simulation system is  $5.430 \times 5.430 \text{ nm}^2$ . (b) Phonon transmittance of Ge thin film (thickness of 0.543 nm, blue dots in inset) sandwiched between crystalline Si leads (red dots in inset). The cross section of the simulation system is  $3.258 \times 3.258 \text{ nm}^2$ .

### III. PHONON KINETICS ANALYSES

We now evaluate the thermal conductivity reduction of the Si/GeND film based on analytical solution of the Boltzmann transport equation (BTE), which is given by

$$\kappa = \frac{1}{3V} \sum_{\mathbf{k},s} C_{\mathbf{k},s} v_{\mathbf{k},s}^2 \tau_{\mathbf{k},s}, \quad (1)$$

where  $V$  is the volume of the primitive unit cell,  $s$  is the branch of phonons,  $\mathbf{k}$  is the wave vector,  $C_{\mathbf{k},s}$  is the mode specific heat of phonons,  $v_{\mathbf{k},s}$  is the group velocity, and  $\tau_{\mathbf{k},s}$  is the relaxation time. Here, phonons are scattered by an anharmonic (three-phonon) scattering process and scattering by the nanostructures including GeNDs and ultrathin  $\text{SiO}_2$  layers. Note that when the anharmonic scattering ( $\tau_{\mathbf{k},s,a}^{-1}$ ) and boundary scattering by the nanostructures ( $\tau_{\mathbf{k},s,\text{NS}}^{-1}$ ) are independent events, the total phonon scattering rate  $\tau_{\mathbf{k},s}^{-1}$  can be calculated by Matthiessen's rule, and thus  $\tau_{\mathbf{k},s}^{-1} = \tau_{\mathbf{k},s,a}^{-1} + \tau_{\mathbf{k},s,\text{NS}}^{-1}$ . Here, inside the Si layer, phonons are assumed to follow the bulk transport properties; the dispersion relations and transport properties  $C_{\mathbf{k},s}$ ,  $v_{\mathbf{k},s}$ , and  $\tau_{\mathbf{k},s,a}$  were obtained by anharmonic lattice dynamics with the first-principles based interatomic force constants with  $30 \times 30 \times 30$  wave-vector mesh. The obtained bulk phonon properties have been confirmed to reproduce the bulk thermal conductivity of a Si crystal, which is  $140 \text{ W m}^{-1} \text{ K}^{-1}$  at room temperature [18].

We model the phonon relaxation time by the nanostructures as  $\tau_{\mathbf{k},s,\text{NS}}^{-1} = v_{\mathbf{k},s}/\Lambda_{\text{NS}}(\omega)$ , where  $\Lambda_{\text{NS}}(\omega)$  is the effective phonon mean free path (MFP) of the Si/GeND film due to the nanostructures. Here, scattering at the surface of the film is negligible because  $\Lambda_{\text{NS}}$  is much smaller than the film thickness. Following the formulation described in Ref. [31],  $\Lambda_{\text{NS}}$  can be determined by the Landauer formula expressed as

$$\Lambda_{\text{NS}}(\omega) = \frac{3}{2} L \int_0^{\pi/2} t_{12}(\theta, \omega) \cos \theta \sin \theta d\theta, \quad (2)$$

where  $t_{12}$ ,  $L$ , and  $\theta$  are the frequency-dependent transmission probability of phonons through the structure, length of the system, and angle of incident phonons, as shown in Fig. 4(a). In this study,  $t_{12}$  is obtained by using Monte Carlo ray tracing simulation, and we name  $\Lambda_{\text{NS}}$  calculated by the ray tracing simulation as  $\Lambda_{\text{NS,RT}}$ . The detail of the ray tracing simulation is described by Hori *et al.* [31] but, briefly, the simulation traces a ballistic phonon transport, which is reflected and transmitted at each boundary or interface of the nanostructures according to the local transmission probability  $t_{\text{int}}$ , which is here used to model transmission through the ultrathin  $\text{SiO}_2$  layers. As a result, the phonon emitted from one side of the simulation system (surface 1) is transmitted or reflected to the opposite (surface 2) or same side (surface 1). The transmissivity of the system,  $t_{12}$ , can be obtained from this probability by scanning the phonon incidents over the polar angles  $\theta[0, \pi/2]$  with randomly selected angle  $\varphi$  and the  $xy$  coordinates. Here, we regard our Si/GeND film as a Si superlattice structure with embedded GeNDs, as in the schematic of the simulation cell shown in Fig. 4(b) with the parameters in Table I.

The important ingredients of the above simulation are the scattering or transmission models of the GeNDs and ultrathin  $\text{SiO}_2$  layers. As for the scattering model of the GeNDs, we first assume that phonons are diffusely scattered at boundaries between a GeND and surrounding Si; i.e., surface specularity is equal to zero. This is reasonable for phonon scattering for the current temperature range and is also supported by previous quantitative reproduction of Si-nanocrystal thermal conductivity with diffuse boundary scattering [31,32]. One key simplification made here is to assume GeNDs as a nanovoid of the same volume, as has been done for nanoinclusions in PbTe [33]. The validity of the simplification is investigated by performing the phonon transmittance calculation of GeNDs embedded in Si by the atomistic Green's function (AGF) method [34,35]. As described in Fig. 3(a), a Ge hemisphere 3.258 nm in diameter (blue dots in the inset) was embedded in a Si (red dots) crystal. The cross section

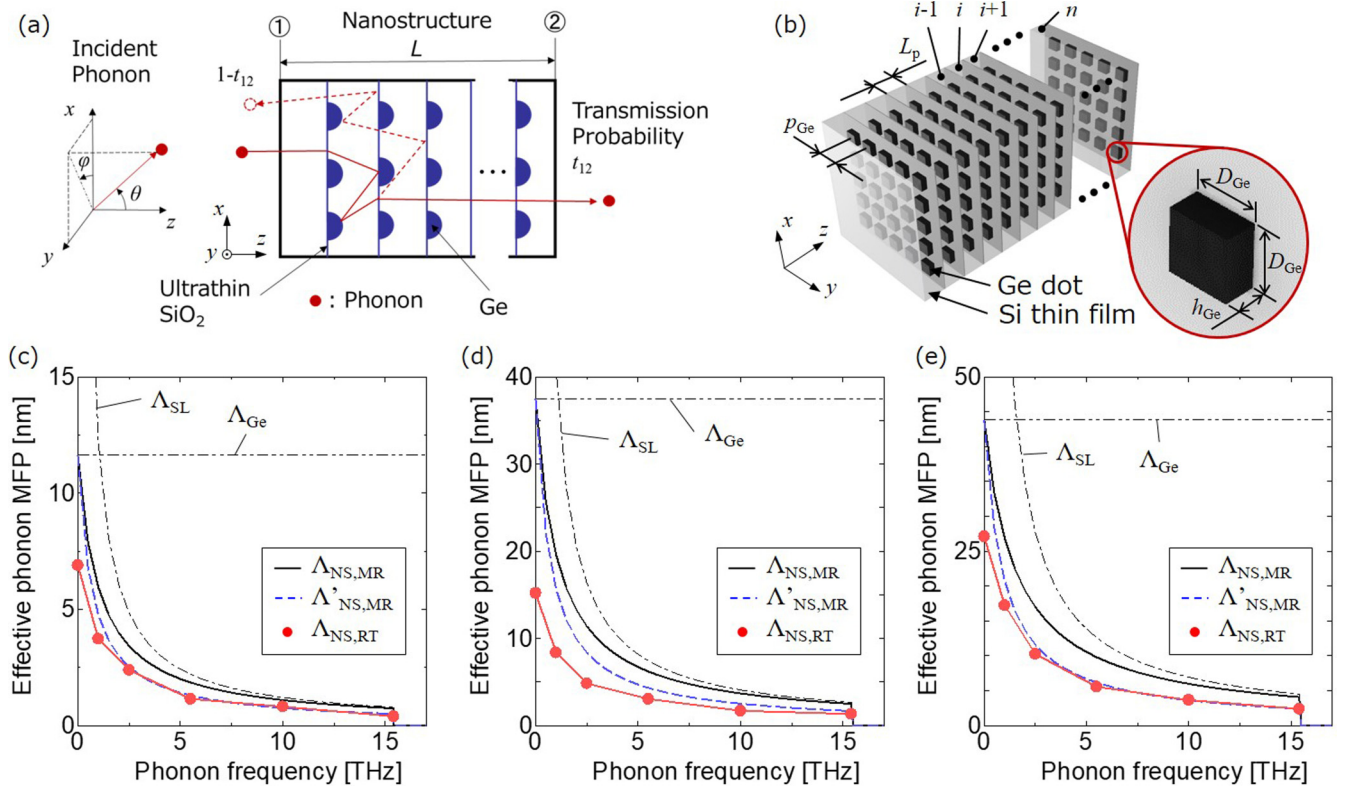


FIG. 4. Monte Carlo ray tracing calculations. (a) A schematic of the Monte Carlo ray tracing calculation. (b) Si/GeNDs model with cubic GeNDs for the calculation.  $D_{\text{Ge}}$  and  $h_{\text{Ge}}$  are considered equal to  $L_{\text{Ge}}$  and  $L_{\text{Ge}}/2$ , respectively, where  $L_{\text{Ge}}$  is the lateral dot size of Ge in Table I. (c)–(e) represent effective phonon mean free path of 5-nm NDs, 40-nm NDs, and 13-nm NDs, respectively.  $\Lambda_{\text{SL}}$ ,  $\Lambda_{\text{Ge}}$ , and  $\Lambda_{\text{NS,RT}}$  denote the MFPs of the Si superlattice, GeNDs, and Si/GeND structure calculated by the ray tracing calculations.  $\Lambda_{\text{NS,MR}}$  and  $\Lambda'_{\text{NS,MR}}$  represent the MFP calculated by Matthiessen's rule ( $1/\Lambda_{\text{NS,MR}} = 1/\Lambda_{\text{SL}} + 1/\Lambda_{\text{Ge}}$ ) and modified Matthiessen's rule ( $1/\Lambda'_{\text{NS,MR}} = 1/\Lambda_{\text{SL}} + 1/[t_{\text{int}}(\omega)\Lambda_{\text{Ge}}]$ ), respectively.

of the simulation system is  $5.430 \times 5.430 \text{ nm}^2$ . The harmonic terms of the Stillinger-Weber potential were used for the force fields of these calculations both for Si and Ge [36]. The AGF calculation was performed for a  $10 \times 10$  wave-vector mesh in the cross section. The calculation was also done for the nanovoid by deleting the Ge atoms. The obtained transmittance spectra over the frequency are shown in Fig. 3(a). The calculations reveal that the spectra of the GeND and nanovoid are similar with a moderate difference in the lower half of the frequency range. One notable feature in both transmittances is that the frequency dependence above 1 THz, the frequency above which phonons contribute to thermal conductivity, is weak. This is compared with the case of a Ge thin film with a thickness of 0.543 nm (blue dots in inset) shown in Fig. 3(b), where the transmission is zero above 11 THz due to cutoff of Ge density of states and has some peaks caused by the resonance due to the Ge thin layer. The absence of this steep decrease with increasing frequency and the resonance peaks in Fig. 3(a) indicates that the major phonon transport paths in the GeND system are through the Si matrix, which should be why the nanovoid model reasonably reproduces the transmission. Therefore, since the size of GeND can be as large as 40 nm, which is too large to perform the AGF calculation, we approximated the GeND with the nanovoid. Furthermore, we have also checked that the actual shape of

the void is not important as long as the scattering cross section and the number density is the same in determining the phonon transmittance, and thus we have adopted the cuboid shape as shown in Fig. 4(b) in the Monte Carlo ray tracing simulation for simplicity. The ray tracing calculation with cuboid shape agrees well with the theoretical model [37–39] of spherical voids distributed uniformly,  $\Lambda^{-1} = 2\pi R^2 n$ , where  $R$  and  $n$  are radius and number density of voids.

As for the phonon transmittance through the ultrathin  $\text{SiO}_2$  layers, phonons are transmitted and reflected with the local transmissivity  $t_{\text{int}}$ . In general, the transmission function across the interface between the sample materials, as in the current case between Si and Si, is modeled as [18,32]

$$t_{\text{int}}(\omega) = \frac{1}{\gamma\omega/\omega_{\text{max}} + 1}, \quad (3)$$

where  $\gamma$  is a constant value and  $\omega_{\text{max}}$  is the maximum phonon frequency. Here, we employ  $\gamma = 7.45$ , the best-fit value obtained by the atomistic Green's function simulation across a 0.36 nm thick  $\text{SiO}_2$  thin film [18]. Therefore, we adopt Eq. (3) with  $\gamma = 7.45$  as  $t_{\text{int}}$  for the ultrathin  $\text{SiO}_2$  interface in the Monte Carlo ray tracing simulation.

#### IV. SYNERGETIC SCATTERING EFFECT

The effective phonon MFP that includes scattering by both GeNDs and an ultrathin SiO<sub>2</sub> layer ( $\Lambda_{\text{NS,RT}}$ ) obtained by the Monte Carlo ray tracing simulation is shown in Figs. 4(c)–4(e). In order to gain understanding in the mechanism of the reduction in the effective MFP by GeNDs and an ultrathin SiO<sub>2</sub> layer, we compare the effective MFPs with the ones obtained by Matthiessen's rule, which assumes the scattering events to be independent from each other. There, effective MFP is estimated as  $\Lambda_{\text{NS,MR}}^{-1} = \Lambda_{\text{Ge}}^{-1} + \Lambda_{\text{SL}}^{-1}$ , where  $\Lambda_{\text{Ge}}$  and  $\Lambda_{\text{SL}}$  are effective MFPs of the Si system with only GeNDs and only ultrathin SiO<sub>2</sub> layers, respectively, which are calculated separately by the Monte Carlo ray tracing method. Note that  $\Lambda_{\text{SL}}$  can also be calculated as

$$\Lambda_{\text{SL}} = \frac{3}{4} \left[ \frac{t_{\text{int}}(\omega)}{1 - t_{\text{int}}(\omega)} \right] L_{\text{SL}}, \quad (4)$$

where  $L_{\text{SL}}$  is a superlattice periodicity [32].

The significant difference between  $\Lambda_{\text{NS,RT}}$  and  $\Lambda_{\text{NS,MR}}$  in Figs. 4(c)–4(e) clarifies the synergetic scattering effect of GeNDs and ultrathin SiO<sub>2</sub> layers. The mechanism of the synergetic effect is that the phonon particles reflected at the superlattice boundaries experience reciprocating motion within the layer, enhancing the collision rate with the nanodots. To give quantitative support to this mechanism, we estimate how many times the phonons in the  $i$ th layer cross the GeND region before moving to the  $i - 1$ th or  $i + 1$ th layer, as shown in Fig. 4(b). When a phonon reaches the  $i + 1$ th layer without being reflected by SiO<sub>2</sub> layers, the phonon has passed through the Ge region once. When a phonon is reflected once at the SiO<sub>2</sub> interface and reaches the  $i - 1$ th layer, the phonon has passed through the Ge region twice. In this way, the expected value of times crossing through the GeND region before reaching the  $i - 1$ th or  $i + 1$ th layer from the  $i$ th layer is  $1/t_{\text{int}}$ . As a result, the phonon scattering rate of GeNDs with the superlattice becomes  $1/t_{\text{int}}$  times larger than the value without the superlattice. The modified scattering rate by the synergetic effect can be incorporated in the Matthiessen's rule as

$$\frac{1}{\Lambda'_{\text{NS,MR}}} = \frac{1}{t_{\text{int}}(\omega)\Lambda_{\text{Ge}}} + \frac{1}{\Lambda_{\text{SL}}}, \quad (5)$$

and here we call this the modified Matthiessen's rule, and  $\Lambda'_{\text{NS,MR}}$  the modified phonon MFP. This  $\Lambda'_{\text{NS,MR}}$  can explain the reduction of phonon MFP calculated by the ray tracing ( $\Lambda_{\text{NS,RT}}$ ), especially at high frequencies, as shown in Figs. 4(c)–4(e). At the low frequency limit, the modified Matthiessen's rule approaches the original one not the ray tracing calculations. This discrepancy is due to phonon scattering enhancement by the side face of the nanodots caused by diffuse interfaces. The ray tracing calculation takes the directional change of phonons into consideration, resulting in an additional phonon scattering event. This consideration suggests that the modified Matthiessen's rule is suitable to the system with a specular interface.

Together with the obtained  $\Lambda_{\text{NS,RT}}$  and  $\Lambda_{\text{NS,MR}}$ , we can calculate the thermal conductivity of the Si/GeND structure, as shown in Fig. 2. It is remarkable that the phonon gas kinetics calculation using the Monte Carlo ray tracing incorporating

the multiple scattering events at GeNDs and SiO<sub>2</sub> layers well reproduces the thermal conductivity reduction measured by experiments for the entire ranges of temperature and dot size without any fitting parameter. Still, the experimental values are slightly smaller than the calculated values, which could be due to the imperfection of the samples, such as the stacking faults. It should be noted that stacking faults are expected to cause only a small reduction in  $\kappa$  ( $\sim 30\%$   $\kappa$  reduction in bulk fcc crystals) [29]. The relatively larger discrepancy between theory and experiment for the case of 40-nm GeNDs should be because the geometry has a large variance of nanodot size distribution and connected nanodots with high Ge content.

On the other hand, the thermal conductivity obtained using Matthiessen's rule largely underestimates the reduction. This means, in terms of the effective MFPs shown in Figs. 4(c)–4(e), the MFP is significantly overestimated by the Matthiessen's rule; i.e., the scatterings of the GeNDs and SiO<sub>2</sub> layers are not independent. Although the scattering rate of only the GeNDs is much smaller than the SiO<sub>2</sub> interfaces, it significantly influences the phonon scattering at the SiO<sub>2</sub> interfaces. This result agrees well with the discussion in electron transport by Sun *et al.* [40]. They investigated the effect of surface and grain-boundary scattering for the resistivity in Cu thin films through resistivity measurement and quantitative analysis and found that grain-boundary scattering is the dominant scattering source but surface scattering is not negligible, which cannot be explained by Matthiessen's rule.

This is because Matthiessen's rule cannot be applied directly to planar scattering events, i.e., surfaces and grain boundaries, as Landauer indicated [41]. Intrinsic scattering events such as anharmonic scattering, electron-phonon scattering, and impurity scattering can be included as perturbations of the phonon population when solving BTE because scattering events occur everywhere and uniformly in the nanostructure. On the other hand, planar scattering processes are incorporated in the boundary condition of the BTE, and they are local events near the boundary.

This result indicates that NDs can reduce the thermal conductivity efficiently when combined with other surface scattering sources, such as polycrystalline nanostructure. In order to confirm the impact of NDs on polycrystalline nanostructure, we calculate the thermal conductivity of the system with NDs (5 nm in diameter, 30 nm pitch) embedded in a Si polycrystal with grain size of 30 nm at 300 K by the ray tracing simulation, where the grain boundary is treated the same as Si/GeND. Using Matthiessen's rule, reduction in the thermal conductivity is only 10.0% by adding GeNDs. In comparison, the ray tracing calculation reveals that reduction is 18.7%. This result implies that further reduction on the thermal conductivity is possible with the synergistic effect of nanodots and crystalline boundaries. This insight is useful to design the nanostructured thermoelectric materials.

#### V. CONCLUSION

To conclude, we report the thermal conductivity of an epitaxial stacked structure of ultrasmall GeNDs embedded in a Si epitaxial nanostructure in the range of 50 K to room temperature by using the TDTR method. Together with the phonon-gas-kinetics analysis using first-principles, atomistic

Green's function, and Monte Carlo ray tracing simulation that reproduces the measured temperature-dependent thermal conductivity, it is found that phonon scattering rates are largely promoted by the synergistic effect of ultrathin SiO<sub>2</sub> interfaces and GeNDs. There, the scattering rate becomes significantly larger than when applying Matthiessen's rule to the scattering rates of GeNDs and ultrathin SiO<sub>2</sub> interfaces. The synergetic effect arises as the phonons reflect at the superlattice boundaries reciprocally move within the layer and collide more with the GeNDs before exiting the layer. The effect was modeled by the modified Matthiessen's rule which

quantitatively describes the synergetic effect. These results give insights useful for designing thermoelectric materials with low thermal conductivity.

#### ACKNOWLEDGMENTS

Part of this work was financially supported by JSPS KAKENHI (Grant No. 19H00744) and JST CREST (Grants No. JPMJCR20Q3 and No. JPMJCR19I2). T.O. was financially supported by JSPS Fellowship (Grant No. 26-9110).

- [1] G. J. Snyder and E. S. Toberer, *Nat. Mater.* **7**, 105 (2008).
- [2] J. P. Heremans, V. Jovovic, E. S. Toberer, A. Saramat, K. Kurosaki, A. Charoenphakdee, S. Yamanaka, and G. J. Snyder, *Science* **321**, 554 (2008).
- [3] A. J. Minnich, M. S. Dresselhaus, Z. F. Ren, and G. Chen, *Energy Environ. Sci.* **2**, 466 (2009).
- [4] W. M. Yim, E. V. Fitzke, and F. D. Rosi, *J. Mater. Sci.* **1**, 52 (1966).
- [5] Z. H. Dughaish, *Phys. B (Amsterdam, Neth.)* **322**, 205 (2002).
- [6] A. Majumdar, *Science* **303**, 777 (2004).
- [7] K. Biswas, J. He, I. D. Blum, C.-I. Wu, T. P. Hogan, D. N. Seidman, V. P. Dravid, and M. G. Kanatzidis, *Nature* **489**, 414 (2012).
- [8] B. Poudel, Q. Hao, Y. Ma, Y. Lan, A. J. Minnich, B. Yu, X. Yan, D. Wang, A. Muto, D. Vashaee, X. Chen, J. Liu, M. S. Dresselhaus, G. Chen, and Z. Ren, *Science* **320**, 634 (2008).
- [9] M. Kashiwagi, S. Hirata, K. Harada, Y. Zheng, K. Miyazaki, M. Yahiro, and C. Adachi, *Appl. Phys. Lett.* **98**, 023114 (2011).
- [10] M. Takashiri, T. Borca-Tasciuc, A. Jacquot, K. Miyazaki, and G. Chen, *J. Appl. Phys.* **100**, 054315 (2006).
- [11] R. Chen, A. I. Hochbaum, P. Murphy, J. Moore, P. Yang, and A. Majumdar, *Phys. Rev. Lett.* **101**, 105501 (2008).
- [12] G. Joshi, H. Lee, Y. Lan, X. Wang, G. Zhu, D. Wang, R. W. Gould, D. C. Cuff, M. Y. Tang, M. S. Dresselhaus, G. Chen, and Z. Ren, *Nano Lett.* **8**, 4670 (2008).
- [13] S. K. Bux, R. G. Blair, P. K. Gogna, H. Lee, G. Chen, M. S. Dresselhaus, R. B. Kaner, and J. P. Fleurial, *Adv. Funct. Mater.* **19**, 2445 (2009).
- [14] M. Nomura, J. Nakagawa, Y. Kage, J. Maire, D. Moser, and O. Paul, *Appl. Phys. Lett.* **106**, 143102 (2015).
- [15] R. Guo and B. Huang, *Sci. Rep.* **5**, 9579 (2015).
- [16] A. Miura, S. Zhou, T. Nozaki, and J. Shiomi, *ACS Appl. Mater. Interfaces* **7**, 13484 (2015).
- [17] Y. Nakamura, M. Isogawa, T. Ueda, S. Yamasaka, H. Matsui, J. Kikkawa, S. Ikeuchi, T. Oyake, T. Hori, J. Shiomi, and A. Sakai, *Nano Energy* **12**, 845 (2015).
- [18] T. Oyake, L. Feng, T. Shiga, M. Isogawa, Y. Nakamura, and J. Shiomi, *Phys. Rev. Lett.* **120**, 045901 (2018).
- [19] S. Yamasaka, Y. Nakamura, T. Ueda, S. Takeuchi, and A. Sakai, *Sci. Rep.* **5**, 14490 (2015).
- [20] S. Yamasaka, Y. Nakamura, T. Ueda, S. Takeuchi, Y. Yamamoto, S. Arai, T. Tanji, N. Tanaka, and A. Sakai, *J. Electron. Mater.* **44**, 2015 (2015).
- [21] Y. Nakamura, A. Murayama, and M. Ichikawa, *Cryst. Growth Des.* **11**, 3301 (2011).
- [22] Y. Nakamura, A. Murayama, R. Watanabe, T. Iyoda, and M. Ichikawa, *Nanotechnology* **21**, 095305 (2010).
- [23] S. Yamasaka, K. Watanabe, S. Sakane, S. Takeuchi, and A. Sakai, *Sci. Rep.* **6**, 22838 (2016).
- [24] S. Sakane, T. Ishibe, T. Hinakawa, N. Naruse, Y. Mera, M. M. Alam, K. Sawano, and Y. Nakamura, *Appl. Phys. Lett.* **115**, 182104 (2019).
- [25] M. Kashiwagi, Y. Sudo, T. Shiga, and J. Shiomi, *Phys. Rev. Applied* **10**, 044018 (2018).
- [26] D. G. Cahill, *Rev. Sci. Instrum.* **75**, 5119 (2004).
- [27] A. J. Schmidt, X. Chen, and G. Chen, *Rev. Sci. Instrum.* **79**, 114902 (2008).
- [28] B. C. Gundrum, D. G. Cahill, and R. S. Averback, *Phys. Rev. B* **72**, 245426 (2005).
- [29] S.-M. Lee, D. G. Cahill, and R. Venkatasubramanian, *Appl. Phys. Lett.* **70**, 2957 (1997).
- [30] G. Pernot, M. Stoffel, I. Savic, F. Pezzoli, P. Chen, G. Savelli, A. Jacquot, J. Schumann, U. Denker, I. Mönch, C. Deneke, O. G. Schmidt, J. M. Rampnoux, S. Wang, M. Plissonnier, A. Rastelli, S. Dilhaire, and N. Mingo, *Nat. Mater.* **9**, 491 (2010).
- [31] T. Hori, J. Shiomi, and C. Dames, *Appl. Phys. Lett.* **106**, 171901 (2015).
- [32] Z. Wang, J. E. Alaniz, W. Jang, J. E. Garay, and C. Dames, *Nano Lett.* **11**, 2206 (2011).
- [33] T. Hori, G. Chen, and J. Shiomi, *Appl. Phys. Lett.* **104**, 021915 (2014).
- [34] W. Zhang, T. S. Fisher, and N. Mingo, *Numer. Heat Transfer, Part B* **51**, 333 (2007).
- [35] T. Yamamoto and K. Watanabe, *Phys. Rev. Lett.* **96**, 255503 (2006).
- [36] F. H. Stillinger and T. A. Weber, *Phys. Rev. B* **31**, 5262 (1985).
- [37] A. Majumdar, *J. Heat Transfer* **115**, 7 (1993).
- [38] H. Zhang and A. J. Minnich, *Sci. Rep.* **5**, 8995 (2015).
- [39] N. Mingo, D. Hauser, N. P. Kobayashi, M. Plissonnier, and A. Shakouri, *Nano Lett.* **9**, 711 (2009).
- [40] T. Sun, B. Yao, A. P. Warren, K. Barmak, M. F. Toney, R. E. Peale, and K. R. Coffey, *Phys. Rev. B* **81**, 155454 (2010).
- [41] R. Landauer, *IBM J. Res. Dev.* **1**, 223 (1957).